HHS Public Access

Author manuscript

Adv Biol (Weinh). Author manuscript; available in PMC 2022 January 04.

Published in final edited form as:

Adv Biol (Weinh). 2021 January ; 5(1): e2000176. doi:10.1002/adbi.202000176.

Enhancement of Wound Healing Efficacy by Increasing the Stability and Skin-Penetrating Property of bFGF Using 30Kc19α-Based Fusion Protein

Haein Lee[†], **Young-Hyeon An**[†], **Tae Keun Kim**, **Jina Ryu**

School of Chemical and Biological Engineering, Institute of Chemical Processes, Seoul National University, 1 Gwanak-ro, Gwanak-gu, Seoul 08826, Republic of Korea

G. Kate Park,

Interdisciplinary Program in Bioengineering, Seoul National University, 1 Gwanak-ro, Gwanak-gu, Seoul 08826, Republic of Korea

Gordon Center for Medical Imaging, Department of Radiology, Massachusetts General Hospital and Harvard Medical School, Boston, MA 02114, USA

Mihn Jeong Park

Interdisciplinary Program in Bioengineering, Seoul National University, 1 Gwanak-ro, Gwanak-gu, Seoul 08826, Republic of Korea

Junghyeon Ko, **Hyunbum Kim**

School of Chemical and Biological Engineering, Institute of Chemical Processes, Seoul National University, 1 Gwanak-ro, Gwanak-gu, Seoul 08826, Republic of Korea

Hak Soo Choi

Gordon Center for Medical Imaging, Department of Radiology, Massachusetts General Hospital and Harvard Medical School, Boston, MA 02114, USA

Nathaniel S. Hwang, **Tai Hyun Park**

School of Chemical and Biological Engineering, Institute of Chemical Processes, Seoul National University, 1 Gwanak-ro, Gwanak-gu, Seoul 08826, Republic of Korea

Interdisciplinary Program in Bioengineering, Seoul National University, 1 Gwanak-ro, Gwanak-gu, Seoul 08826, Republic of Korea

BioMAX/N-Bio Institute, Institute of BioEngineerig, Seoul National University, 1 Gwanakro, Gwanak-gu, Seoul 08826, Republic of Korea

Abstract

nshwang@snu.ac.kr (N. S. Hwang) and thpark@snu.ac.kr (T. H. Park).
[†]H. Lee and Y.-H. An contributed equally to this work.

Supporting Information

Supporting Information is available from the Wiley Online Library or from the author.

Conflict of interest

The authors have declared that no competing interest exists.

The instability of recombinant basic fibroblast growth factor (bFGF) is a major disadvantage for its therapeutic use and means frequent applications to cells or tissues are required for sustained effects. Originating from silkworm hemolymph, 30Kc19α is a cell-penetrating protein that also has protein stabilization properties. Herein, it was investigated whether fusing 30Kc19α to bFGF could enhance the stability and skin penetration properties of bFGF, which may consequently increase its therapeutic efficacy. The fusion of 30Kc19α to bFGF protein increased protein stability, as confirmed by ELISA. 30Kc19α-bFGF also retained the biological activity of bFGF as it facilitated the migration and proliferation of fibroblasts and angiogenesis of endothelial cells. It was discovered that 30Kc19α could improve the transdermal delivery of a small molecular fluorophore through the skin of hairless mice. Importantly, it increased the accumulation of bFGF and further facilitated its translocation into the skin through follicular routes. Finally, when applied to a skin wound model *in vivo*, 30Kc19α-bFGF penetrated the dermis layer effectively, which promoted cell proliferation, tissue granulation, angiogenesis, and tissue remodeling. Consequently, our findings suggest that 30Kc19α improves the therapeutic functionalities of bFGF, and would be useful as a protein stabilizer and/or a delivery vehicle in therapeutic applications.

Graphical Abstract

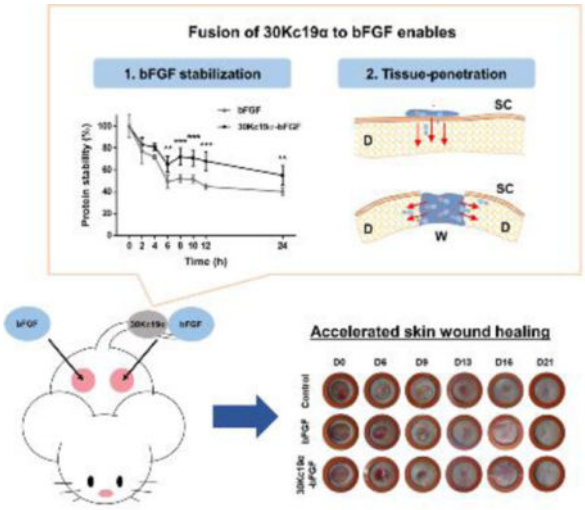

The inherent instability of recombinant basic fibroblast growth factor (bFGF) reduces its effectiveness in clinical use. In this study, 30Kc19α protein was fused to bFGF to solve this problem. 30Kc19α-bFGF has more stable characteristics than bFGF. Furthermore, it shows skin tissue penetration ability. When applied to an *in vivo* wound model, 30Kc19α-bFGF shows excellent skin tissue regeneration, which could be achieved via enhanced stability and facilitated dermal tissue penetration.

Keywords

basic fibroblast growth factor (bFGF); cell-penetrating protein; protein stabilizer; transdermal delivery; skin wound healing

1. Introduction

Basic fibroblast growth factor (bFGF), a member of the fibroblast growth factor (FGF) family, is known for its versatile involvement in tissue growth and regeneration, including wound healing. Activation of FGF receptor by bFGF stimulates intracellular signaling pathways such as phosphoinositide 3-kinase (PI3K)/protein kinase B (Akt) and mitogen-activated protein kinase (MAPK)/extracellular signal-regulated kinase (ERK) signaling pathways which are related to the mitogenic response of cells.[1] As bFGF acts on various target cells involved in wound healing, its effects on wound healing have been extensively studied.[2] bFGF promotes the migration of dermal fibroblasts, keratinocytes, and endothelial cells, into wound sites and facilitates their proliferation.[3] As a result, bFGF accelerates granulation tissue formation and angiogenesis, which results in matrix formation and remodeling.[4]

In recent years, a number of clinical uses of recombinant bFGF have been reported, and these include treatment of chronic wounds, second-degree burns, pressure ulcers, and diabetic foot ulcers.[5] However, its inherent instability and rapid degradation often require frequent treatments in tandem with higher concentrations.[6] The reported half-life of recombinant bFGF is less than 10 hours under normal cell culture conditions and even shorter in the living organisms, which significantly limits its bioavailability in both *in vitro* and *in vivo* applications.[7] Therefore, molecular biotechnological methods to enhance the stability of the bFGF would improve its clinical use. In earlier studies, stabilization of bFGF was attempted by introducing mutations or structural modifications to the molecule or by utilizing heparin for bFGF protection.[8]

Here we have attempted to solve the problem of recombinant bFGF instability by using the 30Kc19α protein, which is an α-helix domain of 30Kc19. Since silkworm hemolymph exhibited anti-apoptotic effects in various cell systems, 30K protein family members, were isolated from silkworm hemolymph and studied intensively.[9,10] Among them, 30Kc19 received attention for its anti-apoptotic and protein stabilizing effects.[11] It was also discovered that 30Kc19 possessed cell- and tissue- penetrating properties by virtue of containing a type of cell-penetrating peptide (CPP) named Pep-c19.[12] In our previous work, we confirmed that the 30Kc19α retains important functions exhibited by 30Kc19.[13] 30Kc19α enhanced stability of cargo proteins and provided functional moieties for cell- and tissue-penetration when it was fused to green fluorescent protein (GFP).[14] Based on these unique properties, we investigated whether the fusion of 30Kc19α to bFGF could enhance the stability of bFGF by protecting it from degradation. In addition we assessed whether the fusion of 30Kc19α would enable transdermal delivery and/or improve the dermal tissue permeability of bFGF. We finally investigated the tissue-regenerative ability of the fusion protein by applying it to an *in vivo* skin wound model in mice. Our data highlights the potential of using 30Kc19α in tissue regeneration through improving both the stability and tissue penetration of biomolecules.

2. Results

2.1. The Fusion of 30Kc19α to bFGF Enhances Stability, Cell Surface Deposition, and Cell-Penetration

N-terminal amino acids of bFGF are flexible and not involved in the interaction with FGFR. Therefore, we fused 30Kc19α to the N-terminus of bFGF.[15] To produce recombinant bFGF and 30Kc19α-bFGF, pET-23a/*bFGF* and pET-23a/*30Kc19α-bFGF* were constructed (Figure 1A and Figure S1, Supporting Information). The plasmids were digested with *Eco*RI and *Xho*I for reconfirmation and the lengths of restricted portions were within their theoretical values. Recombinant proteins were expressed in *E. coli* and purified by FPLC. Western blot analysis showed that the sizes of purified proteins corresponded to the predicted sizes of bFGF and 30Kc19α-bFGF, which are 17.2 and 27.4 kDa, respectively (Figure 1A). Next, the effect of 30Kc19α on the stability of bFGF was assessed by comparing the rate of bFGF degradation. The stability of 30Kc19α-bFGF in solution at 37°C tended to decrease for the first 6 hours of incubation but remained stable beyond this point (Figure 1B). In contrast, bFGF was less stable and decreased over time, reaching 50% within 6 hours.

Prior to treating cells with recombinant proteins, LIVE/DEAD viability assay and CCK-8 assay were performed to test their cytotoxicity. A similar number of red fluorescence (EthD-1) was observed in the three groups and the cell viability of both bFGF- and 30Kc19α-bFGF-treated HDFs were nearly 100% compared to the control group, indicating non-cytotoxic features of the recombinant proteins (Figure 1C and 1D).

Since the 30Kc19α has been previously reported to exhibit cell-penetrating abilities, intracellular translocation of 30Kc19α-bFGF was visualized via confocal laser scanning microscopy (CLSM) after immunofluorescence staining and compared to that seen with bFGF (Figure 1E). Equimolar recombinant bFGF and 30Kc19α-bFGF proteins were applied to HDFs for 4 hours, followed by fixation and immunostaining with an anti-T7 tag antibody. The green-fluorescent T7 tag was observed in bFGF and 30Kc19α-bFGF-treated groups; however, the 30Kc19α-bFGF-treated group showed higher fluorescence on both the cell surface and in the cytosol of HDFs than the bFGF-treated group. This suggests that the fusion of 30Kc19α to bFGF enhanced protein stability and cellular uptake.

2.2. Enhanced bFGF Stability Improves Mitogenic Functions of bFGF

Higher stability means prolonged bioactivities of bFGF. Thus, it is assumed that higher mitogenic effects are produced in cells via prolonged bioactivities of bFGF. Mitogenic functions (cell proliferation and migration) of 30Kc19α-bFGF were evaluated in HDFs, as HDFs constitute the major cell type of the dermis. Firstly, HDF proliferation was measured. Cells were treated with either bFGF or 30Kc19α-bFGF under serum-deficient conditions for 48 hours. The relative proliferation of 30Kc19α-bFGF-treated cells was significantly higher than that of control and bFGF-treated groups (Figure 2A). Proliferative behaviors were also investigated at different protein concentrations (Figure S2, Supporting Information). The 30Kc19α-bFGF-treated group showed more proliferative behavior than the bFGF-treated group when the concentration was below 20 μM; however, adding excess growth factors (100 μM) did not induce greater proliferation but did narrow the difference between bFGF

and the conjugated form. Since 4 μM of 30Kc19α-bFGF showed the highest efficiency, we used that concentration in subsequent experiments.

Next, we carried out *in vitro* wound healing (scratching) assay[16] to investigate the mitogenic effects of 30Kc19α-bFGF. Under wounded conditions, bFGF facilitates the proliferation and migration of cells.[17] Therefore, we hypothesized that enhancing the stability of bFGF using 30Kc19α would increase the rate of gap closure and this was indeed the case. 30Kc19α-bFGF promoted the proliferation and migration of HDFs, which resulted in faster gap closure compared to bFGF until 48 hours (Figure 2B). The percent gap closure of the control, bFGF, and 30Kc19α-bFGF-treated groups after 24 hours were 11.0 ± 2.7, 15.9 ± 3.0, and 23.5 ± 2.2%, respectively, and after 48 hours, 18.3 ± 1.6, 25.2 ± 3.9, and 41.2 ± 5.2%, respectively (Figure 2C). These data indicate that the enhanced stability of 30Kc19α-bFGF improved both proliferation and migration of HDFs.

2.3. 30Kc19α-bFGF Improves the Angiogenic Ability of HUVECs

Exogenous delivery of bFGF has proven to enhance the angiogenesis during wound repair despite its low accumulation at wound sites.[18] We investigated that the enhanced stability and cellular interaction of 30Kc19α-bFGF could improve the angiogenic ability *in vitro* using human umbilical vein endothelial cells (HUVECs). The HUVECs treated with 30Kc19α-bFGF showed improved angiogenic performance, which exhibited both higher tube formation and branching points (Figure 3A). The quantitative analysis represented that 30Kc19α-bFGF significantly supported the tube formation ability of HUVECs than bFGF, and the cells treated with 30Kc19α-bFGF displayed larger numbers of branching points than bFGF (Figure 3B and 3C). This indicates that 30Kc19α protein can improve the angiogenic functionality of bFGF *in vitro* and 30Kc19α-bFGF has the potential to improve the neovascularization during the wound healing process.

2.4. 30Kc19α Elicits Transdermal Transport of NIR Fluorophore *In Vivo*

Among cell membrane-penetrating peptides, some kinds display effective skin penetrating ability by destabilizing the stratum corneum (SC) and/or by macropinocytosis.[19] Given that 30Kc19α contains a cell-penetrating moiety named Pep-c19, we assessed whether the 30Kc19α can penetrate the SC by modifying it with near-infrared (NIR) dye, ZW800–1C, for direct visualization when applied on hairless mouse skin.[12c] Initially, NHS-ester-containing ZW800–1C was conjugated to the amine group in 30Kc19α, followed by formulating with carbomer gel that could be observed under NIR fluorescent microscopy (Figure 4A). We applied the samples into the silicone adhesive isolators, and the samples were washed off and imaged after 4 hours. In the magnified images, ZW800–1C alone exhibited much weaker fluorescent signals than the 30Kc19α conjugated form (Figure 4B). Image quantification showed that ZW800–30Kc19α had a 3.7-fold higher fluorescent intensity compared to ZW800 (Figure 4C). This result shows that 30Kc19α enhanced the skin permeability of small molecules and exhibited potency as a skin penetrating protein.

2.5. 30Kc19α Facilitates the Transdermal Delivery and Dermal Tissue Penetration of bFGF

It is still challenging to deliver therapeutic proteins by transdermal route, but transdermal- or dermal delivery is a promising technique for facile administration and can promote the

wound healing process.[20] After verifying the skin permeability of 30Kc19α using the NIR probe, we wished to determine whether 30Kc19α can deliver bFGF protein transdermally. When applied to hairless mouse skin *in vivo*, we observed the proteins by immunofluorescent staining on both intact skin and in an open wound (Figure 5). 30Kc19α-bFGF indicated strong fluorescent signals at the SC, while bFGF showed slight deposition at the SC. However, we did not observe any penetrant proteins into the dermis layer in either group. In the situation with an open wound, we found that 30Kc19α-bFGF penetrated the dermis layers where the fluorescent signals could be observed between DAPI stains, but there was a little fluorescent signal from bFGF. Since it was difficult to stain bFGF in unsectioned tissues, we applied 30Kc19α-GFP instead of 30Kc19α-bFGF to the wound site to orthogonally observe tissue penetration via CLSM. GFP is a 26.9 kDa protein which exhibits green fluorescence when exposed to blue light. The data showed that a significantly high level of GFP was accumulated into the skin tissue when fused to 30Kc19α (Figure S3, Supporting Information). It suggests that the 30Kc19α could enhance the dermal tissue penetration of bFGF, but the transdermal delivery of 30Kc19α-bFGF was restricted in hairless mice skin.

To further investigate, we carried out tests using *ex vivo* porcine skin (Figure S4, Supporting Information). In the transdermal delivery test, we hypothesized that the existence of the hair follicles might promote the transdermal delivery of 30Kc19α-bFGF. As a result, we could observe that 30Kc19α-bFGF group was observed in the epidermis layer of the skin, on the other hand, the bFGF was shown just in the SC, which indicated 30Kc19α-bFGF could penetrate the intact skin in the existence of hair follicles. Furthermore, at the open wound, 30Kc19α-bFGF exhibited much higher tissue penetration than bFGF alone. The results showed that 30Kc19α could improve not only the transdermal delivery of bFGF through the follicular route but also by dermal tissue penetration.

2.6. 30Kc19α-bFGF Promotes *In Vivo* Wound Healing by Stimulating Cell Proliferation

We evaluated the wound healing effect of 30Kc19α-bFGF in the mouse skin defect model. Carbomer gel was used to retain the samples at the wound site, and PBS-loaded carbomer gel was used as a control group. In the macroscopic analysis, 30Kc19α-bFGF effectively promoted wound regeneration from day 6, and the wound size was significantly reduced on day 8 (Figure 6A and 6B). These regenerative profiles were supported by Ki67 immunofluorescence on day 6. The highest number of proliferative cells were seen with 30Kc19α-bFGF (Figure 6C and 6D). In particular, strong Ki67 signals could be observed in epidermal regions. As a result, it was confirmed that the 30Kc19α-bFGF effectively enhanced the wound healing rate at the macroscopic scale.

2.7. 30Kc19α-bFGF Enhances *In Vivo* Wound Regeneration, Collagen Deposition, and Angiogenesis

The tissue formation and remodeling processes are a critical phase during wound healing, which can determine the quality of the rehabilitated skin, and bFGF is involved in several biological responses, such as collagen deposition and angiogenesis.[21] Thus we qualitatively assessed the regenerative capability of 30Kc19α-bFGF from the histological analysis. Hematoxylin and Eosin (H&E)-stained images of the cross-sectioned tissues were observed,

and the panniculus gap, which is the distance between newly formed panniculus adiposus at wound edges, was measured. On day 6, both the narrow panniculus gap and thick granulation tissue were observed with 30Kc19α-bFGF (Figure S5, Supporting Information). On day 14, both the bFGF and 30Kc19α-bFGF groups showed greater wound healing ability compared to control, but 30Kc19α-bFGF had the narrowest panniculus gap (Figure 7A). On day 21, with 30Kc19α-bFGF treatment, the tissue was being regenerated in the form of a native tissue-resembling structure with a significantly decreased panniculus gap and newly formed appendages (Figure 7B). Specifically, the panniculus gap was further decreased below 100 μm in 30Kc19α-bFGF, whose value was substantially lower than that of both control and bFGF.

Next, we analyzed collagen deposition from Masson's Trichrome (MTC)-stained images. The granulation tissue area of bFGF and 30Kc19α-bFGF were 1.8- and 2.3-fold more substantial than the control group; that is, 30Kc19α-bFGF effectively promoted tissue granulation during wound healing better than bFGF (Figure 8A). From day 14, the skin appendages were being formed and regenerated from the epidermal layer, and there were more as well as better matured appendages observed in 30Kc19α-bFGF than bFGF (Figure S6, Supporting Information). On day 21, the magnified MTC images showed that 30Kc19α-bFGF accelerated much higher collagen deposition and the formation of the skin appendages, such as hair follicles, compared to control and unconjugated bFGF (Figure 8B). In addition, the organization of extracellular matrix (ECM) fiber alignment was measured at the dermal layer. The lower coherence of 30Kc19α-bFGF indicated that the wound was being regenerated toward something more resembling healthy skin tissue. This will be discussed in the following section.

Finally, the angiogenic ability of 30Kc19α-bFGF was evaluated. The skin tissues were stained for alpha-smooth muscle actin (α-SMA) on day 14. Based on the high-power field (HPF) images in the regenerated regions, the highest number of newly formed blood vessels were observed in 30Kc19α-bFGF (Figure 9). More specifically, 30Kc19α-bFGF had a 2.6- and a 1.4-fold higher number of vessels than that of control and bFGF, respectively. Furthermore, it was shown that the vessels in 30Kc19α-bFGF increased not only in number but they were also more stretched and had an enlarged shape compared to bFGF.

3. Discussion

In recent years, several studies have tried to enhance bFGF protein stability. Despite therapeutic effects, bFGF has certain limitations such as short half-life, which means a lack of stability and loss of bioactivity even at room temperature. Stabilization of bFGF can improve its bioactivity and wound healing capacity in the wound environment.[8a] Among the most promising, biomimetic polymeric scaffolds can be used for overcoming the unstable nature of bFGF.[22] For example, Wu *et al.* stabilized the growth factors (GFs) within a heparin-based hydrogel structure, allowing them to be protected from the harsh wound environment, including such threats as enzymatic degradation. However, these scaffold-based approaches do not directly improve the intrinsic stability of bFGF, but indirectly affect the proteins functionalities. Another approach involving disulfide engineering of proteins has also been utilized to introduce added stability.[23] Choi *et al.*

demonstrated that a stabilized bFGF promoted greater wound healing capacity in diabetic mice compared to commercially available bFGF.[8a] However, in this method, additional chemical processes are required. Here we investigated enhancing bFGF stability by fusing 30Kc19α to bFGF. Our results show that bFGF stability as a fusion protein was significantly enhanced. This is in line with previous findings demonstrating that the 30Kc19α has protein-stabilizing effects, whose underlying mechanism has not been fully understood, but for which shielding effects may be derived from hydrophobic interactions between 30Kc19α and bFGF.[11c] The adjacent location of 30Kc19α may reduce the likelihood of bFGF being degraded by proteolytic enzymes. Another possibility is that 30Kc19α may have unknown intrinsic stabilizing sequences. A study by Takano *et al.* demonstrated that the fusion of C-terminal residues of Sto-RNase HI to other proteins resulted in more stable chimeric proteins.[24] For *in vivo* application, it was demonstrated that biomaterials could be deliberately chosen for GF-based wound regeneration based on GF structural considerations, such as ionic properties, surface charges, and binding sites.[25] We chose the carbomer under the assumption that it plays a role not only in retaining the proteins at wound sites but also in providing an electrostatic binding moiety to positively charged bFGF due to its intrinsic anionic nature.

HDFs treated with 30Kc19α-bFGF showed more on the cell surface as well as in the cytosol, than bFGF (Figure 1E). Surface deposition occurs prior to cell penetration. Since bFGF is a kind of receptor-binding protein, bFGF-deposition to the cell surface can increase the localization of proteins to receptors, which means that there is a higher chance of interactions between bFGF and FGFR. In previous studies, the CPP, trans-activator of transcription (TAT), was applied to the intracellular delivery of bFGF.[26] The deposition of bFGF on cell membranes by TAT increased the localization of proteins to receptors, increasing the effect of bFGF on hypertrophic scars. Although the effects of 30Kc19α on the receptor binding of cargo protein has not been studied, 30Kc19α is thought to increase the efficiency of interactions between bFGF and FGFR. Cell penetration of bFGF leads to tissue penetration of bFGF. Facilitated dermal tissue penetration can promote the wound healing process since bFGF can act on cells in deeper dermal tissue. Thus, both surface deposition and cell penetration are significant in the aspect of drug efficacy on wound healing.

Although 30Kc19α has been known as a CPP, the potential of its skin permeability has not been investigated. In general, proteins have limited skin-penetration ability due to its intrinsic hydrophilic and macromolecular features.[20, 27] A lot of enhancement strategies have been developed for delivering proteins into the skin, such as chemical penetration enhancers, cell- or skin-penetrating peptides, nanocarriers, physical penetration enhancers, and microneedle.[27b,28] For delivering bFGF into the skin, Zeng *et al.* used TAT to enable transdermal delivery of aFGF and bFGF, and expand the wound area where aFGF and bFGF can act.[26,29] More recently, Xu *et al.* reported that a permeation enhancer-inserted liposome improved stability and skin-permeability of bFGF.[30] Here, our findings verified that 30Kc19α improved the skin penetration of bFGF and expanded its potential for use as a skin-penetrating protein for delivering small molecules and/or macromolecules transdermally. Despite the relatively large molecular weight of 30Kc19α (12.4 kDa), our finding that the skin permeability of an NIR fluorophore was increased through the conjugation with 30Kc19α was an encouraging result.

The skin-penetration mechanisms of other chemical penetration enhancers have been generally explained according to several modes of action, however, the transport mechanism of CPPs have not been fully explained yet.[25,26] A surface charge mediated transporting mechanism has been suggested for arginine-rich CPPs (positively charged) that interact with skin cells whose surface is negatively charged, followed by skin penetration through transcellular, appendage, and intracellular routes.[29] Hou *et al.* reported that micropinocytosis and actin rearrangement were involved in transdermal delivery of proteins.[19] We investigated the lipid structure of SC treated with bFGF or 30Kc19α-bFGF via X-ray scattering, but there were no distinct peak changes in small-angle or wide-angle regions, demonstrating that 30Kc19α-bFGF may penetrate the skin without altering the lipid organization (Figure S7, Supporting Information).[32] It is possible that the penetration of 30Kc19α might follow the aforementioned mechanisms of CPPs; nevertheless, further work will be needed to identify how 30Kc19α acts at the molecular level to make cargo protein permeable to the skin.

The applicability of 30Kc19α-bFGF to wound healing has been confirmed in several aspects. The protein stability and cell-membrane deposition and penetration were enhanced through the fusion with 30Kc19α, followed by improving functions such as cell proliferation and migration rate of HDFs. Based on the wound healing potential of 30Kc19α-bFGF seen with HDFs and HUVECs, we investigated its efficacy on a wound model in mice. We analyzed the regenerative behavior of 30Kc19α-bFGF, focusing on proliferation and tissue remodeling.[21] Through Ki67-staining, it was confirmed that 30Kc19α-bFGF facilitated proliferation during wound healing to a greater extent than native bFGF. Moreover, a large granulation tissue area provided evidence that 30Kc19α-bFGF continuously influenced the proliferation and infiltration of cells within the surrounding tissue. If the proliferative phase persists, the wound subsequently becomes scar tissue.[33] Therefore, the tissue remodeling process, which includes ECM rearrangement, angiogenesis, and reformation of skin appendages, is essential for wound repair and recovery of skin tissue functionality. ECM fiber organization is one of the criteria used to determine whether regenerated skin resembles native skin tissue. In general, healthy skin has a basketweave orientation.[34] 30Kc19α-bFGF regenerated the dermal layer with low coherence in ECM fiber alignment (Figure 8), suggesting that it promoted wound repair as well as wound closure. Furthermore, angiogenesis is another critical element of wound healing since it controls the quality of skin tissue after regeneration, and bFGF is deeply involved in angiogenesis.[35] During the proliferative phase (day 14), we observed that vessel formation in the wound bed occurred most actively in the 30Kc19α-bFGF group, followed by maturation during remodeling (day 21, Figure S8, Supporting Information). As a result, based on wound size reduction profile and other microscopic analyses, we conclude that 30Kc19α enhanced and boosted the ability of bFGF to facilitate wound regeneration both quantitatively and qualitatively.

4. Experimental Section

Plasmid Construction of bFGF and 30Kc19α-bFGF:

Primers containing specific restriction enzyme recognition sequences were designed to insert *30Kc19α* gene and *bFGF* gene into a pET-23a expression vector (Novagen, USA), as shown in Figure 1A. The primers for 30Kc19α contained *Bam*HI and *Eco*RI, on the N and C terminals, respectively. The primers for bFGF contained *Eco*RI and *Xho*I sites, on the N and C terminals, respectively. PCR was conducted, then the PCR products and pET-23a expression vectors were digested with the appropriate restriction enzymes to create the pET-23a/30Kc19α and pET-23a/bFGF constructs. The constructs were digested *Eco*RI and *Xho*I, and the digested *bFGF* was inserted to pET-23a/*30Kc19α*, to create the pET-23a/*30Kc19α-bFGF* construct.

Protein Expression and Purification of bFGF and 30Kc19α-bFGF:

pET-23a/*bFGF* and pET-23a/*30Kc19α-bFGF* were transformed into BL21 competent cells (Novagen) for protein production. The transformed *E. coli* was cultured in Luria-Bertani (LB) medium (Miller, USA) with 100 μg/ml ampicillin (Sigma-Aldrich, USA) at 37°C overnight with shaking. The LB medium was transferred to 1 L LB medium and cultured at 37°C. When OD_{600} reached between 0.4 and 0.6, 1 mM isopropyl β-D-thiogalactopyranoside (IPTG; Calbiochem, USA) was added to induce protein production, and *E. coli* was further incubated for 4 hours. The cells were harvested by centrifugation and lysed by ultrasonication. The supernatants were filtered, and His-tag affinity chromatography using His-Trap HP column (GE Healthcare, Sweden) was conducted by fast protein liquid chromatography (FPLC; GE Healthcare). The binding, washing (20 mM Tris, 500 mM NaCl, 50 mM imidazole, pH 8.0), and elution (20 mM Tris, 500 mM NaCl, 350 mM imidazole, pH 8.0) buffers were used for protein purification. Buffer was changed to sodium bicarbonate buffer (44 mM sodium bicarbonate, 110 mM NaCl, pH 8.0) or phosphate-buffered saline (PBS; WelGENE Inc., Republic of Korea) and purified proteins were stored at −80°C until further use.

Immunoblot Analysis:

To identify the purified proteins, SDS-PAGE and western blot were conducted. The purified proteins were mixed with 5x sample buffer (250 mM Tris-HCl, 5% 2-mercaptoethanol, 10% SDS, 0.5% bromophenol blue, 50% glycerol, pH 6.8) prior to loading on a 10% SDS-PAGE gel. The purified products on SDS-PAGE were transferred to a polyvinylidene difluoride (PVDF) membrane for western blot. As the pET-23a vector contains a T7 tag, anti-T7 tag antibody (ab9115, Abcam, UK) and anti-rabbit HRP-conjugated antibody (Millipore, USA) were used to label the purified proteins. Lumina Forte Western HRP substrate (Merck Millipore, USA) was used to visualize proteins on the G-Box Chemi XL system (Syngene, UK).

Protein Stability Assay:

Protein stability was assessed by the human basic FGF DuoSet enzyme-linked immunosorbent assay kit (ELISA; R&D Systems, USA). The quantified proteins were

diluted to 10 nM, which is within the detection range of the kit. The diluted proteins were incubated at 37°C from 0 to 24 hours prior to adding to a 96-well microplate (R&D systems). The absorbance was measured at 450 nm by Spark 10M (Tecan, Switzerland).

Cytotoxicity Assay:

HDFs were seeded on 96-well plates and 48-well plates (Thermo Fisher Scientific, USA) and incubated in DMEM supplemented with 10% FBS and 1% PS at 37°C until they reached ~ 70% confluency. Then, the cells were treated with 4 μM of bFGF and 30Kc19α-bFGF and incubated for 24 and 48 hours. For 96-well plates, cell counting kit (CCK)-8 (Dojindo, USA) was used to assess the cytotoxicity of recombinant proteins for 24 and 48 hour-treated samples. CCK solution (10 μl) was added to each well and incubated for 2 hours. The absorbance was measured at 450 nm by Spark 10M. For 48-well plates, cytotoxicity of the purified proteins were evaluated by LIVE/DEAD kit (Invitrogen). Staining was conducted for 48 hour-treated samples following the manufacturer's instruction. The stained samples were observed via fluorescence microscopy (Olympus, Japan).

Immunofluorescnece staining:

Immunofluorescence staining was conducted to assess cellular penetration. HDFs were seeded on confocal dishes (SPL Life Sciences, Republic of Korea) and incubated with Dulbecco's Modified Eagle Medium (DMEM; WelGENE Inc., Republic of Korea) supplemented with 10% fetal bovine serum (FBS; Gibco, Scotland) and 1% penicillin-streptomycin (PS; Gibco) at 37°C with 5% CO_2 until they reached 30% confluency. Purified proteins at 4 μM were added to cells for 1 hour. The proteins were labeled with Alexa Flour® 488 (Invitrogen, USA), and the nucleus was counterstained with DAPI (Invitrogen). Fluorescence was observed on a Carl Zeiss LSM710 (Zeiss, Germany) confocal laser scanning microscopy.

Cell Proliferation Assay:

Cells (7×10^3 per well) were seeded on a 96-well plate (Thermo Fisher Scientific) and incubated in DMEM supplemented with 10% FBS and 1% PS at 37°C with 5% CO_2 for 6 hours. The media was changed to DMEM with 1% PS for the purposes of cell starvation and cycle synchronization. The cells were treated with purified proteins at 4 μM in DMEM with 0.5% FBS and 1% PS and incubated for 24 and 48 hours. Then, CCK-8 assay was performed in the same way as above.

In Vitro Wound Healing (Scratching) assay:

HDFs were seeded on 6-well plates (Thermo Fisher Scientific) and incubated at 37°C with 5% CO_2 until 100% confluency. A micropipette tip was used to create a straight line scratch on the 6-well plate to create a wound in the cell layer. After washing with Dulbecco's phosphate-buffered saline (DPBS; WelGENE Inc.) twice, the HDFs were serum starved overnight at 37°C with 5% CO_2. Proteins (4 μM) in DMEM with 1% PS were added for 24 and 48 hours. The gap closure was calculated by the following equation.

$$\% \text{ gap closure} = \frac{\text{Number of cells in the boundary}}{\text{Confluent number of cells}} \times 100 \quad (1)$$

In Vitro Angiogenesis Assay:

Human umbilical vein endothelial cells (HUVECs; Lonza, USA) were maintained with endothelial cell basal medium-2 supplemented with EGM™-2 singlequots® (Lonza). The matrigel solution (Geltrex® Matrix Product, Thermo Fisher Scientific) was put into a 24-well plate and gelated at 37℃. HUVECs were seeded onto the matrigel at 5×10^4 cells per well and maintained with a serum-free medium that did not contain both bFGF and vascular endothelial growth factor of EGM™-2 kit. The cells were treated with 4 μM of bFGF and 30Kc19α-bFGF, respectively. After 12 hours, we measured the number of tube formation and branching points based on images using ImageJ (ImageJ Software).

Protein Gel Preparation:

Carbomer (Carbopol 940, Polygel CA, Happycall Co., Ltd., Republic of Korea) was used to apply samples into wounds with increased retention. Carbomer was sterilized via UV irradiation overnight and dissolved in deionized (D.I.) water until the solution became homogenous. Triethanolamine was added to adjust pH and make the gel form. Protein (bFGF and 30Kc19α-bFGF) stocks were mixed with the carbomer gel, and a final concentration of carbomer and proteins were 0.5 w/v % and 5.47 μM, respectively.

Conjugation of NIR Fluorophores to 30Kc19α:

30Kc19α was conjugated to the NHS ester form of NIR fluorophore ZW800–1C, as described previously.[36] Briefly, 20 equivalents of ZW800–1C were added to 30Kc19α in PBS (pH 8.0) and incubated for 3 hours at room temperature with gentle shaking. The reaction mixture was purified using the Mini Bio-Gel P6 desalting column (Bio-Rad).

In vivo Skin Penetration Test of 30Kc19α:

This animal study was performed under the supervision of MGH IACUC and housed in an AAALAC certified facility with approved protocol #2016N000622. Sterilized carbomer was mixed with 5 μM of 30Kc19α-ZW800–1C conjugates or ZW800–1C in D.I. water, and then triethanolamine was added to form gels. Press-to-Seal silicone isolators (S1810, 9-mm diameter, Sigma-Aldrich) were used to apply carbomer mixtures on the back of 8 week-old nude mice (NCRNU). After 4 hours, carbomer mixtures were wahsed off three times with a wet towel. Animals were then imaged using the fluorescence-assisted resection and exploration (FLARE) imaging system with 3.6 mW/cm^2 of 760 nm excitation light and white light (400–650 nm) at 5,500 lux. Through ImageJ software, the fluorescent signals were quantified by the signal-to-background ratio (SBR) and normalized to ZW800–1C values.

In vivo Skin Penetration Test of 30Kc19α-bFGF:

All *in vivo* experimental procedures using 30Kc19α-bFGF were approved by the IACUC of the Seoul National University (SNU-190916-2-1), and the study was performed similarly to

the above-mentioned *in vivo* study of 30Kc19α with eight week male balb/c-nude mice (OrientBio Co., Republic of Korea). For the transdermal delivery test, the protein gels were applied to the dorsal regions of hairless mice and washed off after 4 hours. For the skin wound penetration test, full-thickness wounds were formed on dorsal skin by biopsy punch with a diameter of 6 mm, followed by applying the protein gels to the wounds. After 4 hours, the animals were sacrificed by excess CO_2 exposure, and the skin tissues were processed to perform IFC staining as for *ex vivo* experiments on 30Kc19α.

In vivo Wound Healing Application and Wound Size Quantification:

Eight week male balb/c-nude mice were used for *in vivo* wound healing test. The animals were anesthetized with isoflurane during the surgery. Full-thickness wounds were formed on dorsal skin by biopsy punch with a diameter of 6 mm. Press-to-Seal silicone isolators were used for preventing contractile effects and as reference for measuring the wound size. 30 μl of carbomer gel without proteins (control) or 30 μl of protein gels was applied to the wounds every 2–3 days. All wounds were covered by Tegaderm™ film dressing. Wound size was measured using ImageJ software and quantified as the percentage of remaining size compared to the initial defect area.

Histological Analysis:

Mice were sacrificed at each time point by excess CO_2 exposure, and skin tissue including the wound area was excised, followed by fixation in 4% PFA. The tissues were embedded in paraffin and sectioned. For immunofluorescence (IF), primary antibodies to Ki67 (ab15580, Abcam) and α-smooth muscle actin (α-SMA; ab5694, Abcam) were used, respectively.

In Vivo Proliferative Cell Quantification:

The proliferative cells on day 6 during the wound healing stage were quantified from the fluorescent intensity of both Ki67 and DAPI staining images. The percentage values were calculated by measuring the percentage of Ki67 fluorescence normalized to DAPI using ImageJ software.

Panniculus Gap and Granulation Tissue Area Quantification:

Panniculus gap and granulation tissue thickness were manually measured from Hematoxylin and Eosin (H&E) images Masson's Trichrome images using ImageJ software. The margin of the panniculus gap was assigned as a length between the point where the adipocyte coverage area was terminated. Granulation tissue area was also calculated using ImageJ software.

ECM Fiber Alignment Quantification:

Extracellular matrix (ECM) fiber alignment was quantified using the OrientationJ plugin available on ImageJ software, as described in previous research.[34b] Coherence values (dimensionless) were obtained from the region of interest in MTC images of each sample.

In vivo Vessel Formation Quantification:

Vessel formation was quantified based on the high-power field (HPF) 40X magnified images of α-SMA on day 14. Vessel numbers were counted on at least 15 images and averaged.

Statistical Analysis:

Statistical analysis was conducted by the paired student *t*-test to estimate statistical significance. For all animal experiments, each group had n=5–8, and all data are presented as mean ± standard error of the mean.

5. Conclusion

We fused 30Kc19α to bFGF to overcome the instability problem of recombinant bFGF. Our results indicate that 30Kc19α-bFGF has more stable characteristics than bFGF. Prolonging the biological activities of bFGF resulted in improved wound healing effects in HDFs and HUVECs. The skin penetration ability of 30Kc19α was verified using an NIR fluorophore *in vivo*, and the 30Kc19α-bFGF also showed improved accumulation on the skin and exhibited higher transdermal translocation through follicular routes than bFGF. When applied to an *in vivo* wound model, 30Kc19α-bFGF showed excellent skin tissue regeneration, which could be achieved via enhanced stability and facilitated dermal tissue penetration. Therefore, 30Kc19α-bFGF would be a useful wound healing material in therapeutic applications.

Supplementary Material

Refer to Web version on PubMed Central for supplementary material.

Acknowledgements

This work was financially supported by the Ministry of Science and ICT by the Korean Government (NRF-2017M3A9C6031786). In addition, this work was partly supported by US NIH grant NIBIB (#R01EB022230).

References

[1]. Ornitz DM, Itoh N, Wiley Interdiscip. Rev. Dev. Biol2015, 4, 215. [PubMed: 25772309]

[2]. a)Behm B, Babilas P, Landthaler M, Schreml S, J. Eur. Acad. Dermatol 2012, 26, 812;b)Barrientos S, Stojadinovic O, Golinko MS, Brem H, Tomic-Canic M, Wound Repair Regen. 2008, 16, 585. [PubMed: 19128254]

[3]. a)Kanazawa S, Fujiwara T, Matsuzaki S, Shingaki K, Taniguchi M, Miyata S, Tohyama M, Sakai Y, Yano K, Hosokawa K, PLoS One 2010, 5, e12228; [PubMed: 20808927] b)Song YH, Zhu YT, Ding J, Zhou FY, Xue JX, Jung JH, Li ZJ, Gao WY, Mol. Med. Rep 2016, 14, 3336; [PubMed: 27572477] c)O'keefe EJ, Chiu ML, Payne RE Jr, J. Investig. Dermatol 1988, 90;d)Sogabe Y, Abe M, Yokoyama Y, Ishikawa O, Wound Repair Regen. 2006, 14, 457; [PubMed: 16939574] e)Przybylski M, J. Wound Care 2009, 18, 516. [PubMed: 20081577]

[4]. a)Montesano R, Vassalli J-D, Baird A, Guillemin R, Orci L, Proc. Natl. Acad. Sci. U.S.A 1986, 83, 7297; [PubMed: 2429303] b)Akita S, Akino K, Hirano A, Adv. Wound Care (New Rochelle) 2013, 2, 44; [PubMed: 24527324] c)Sasaki T, J. Dermatol 1992, 19, 664. [PubMed: 1293151]

[5]. a)Uchi H, Igarashi A, Urabe K, Koga T, Nakayama J, Kawamori R, Tamaki K, Hirakata H, Ohura T, Furue M, Eur. J. Dermatol 2009, 19, 461; [PubMed: 19638336] b)Nunes QM, Li Y, Sun C, Kinnunen TK, Fernig DG, PeerJ 2016, 4, e1535; [PubMed: 26793421] c)Akita S, Akino K, Imaizumi T, Hirano A, Wound Repair Regen. 2008, 16, 635. [PubMed: 19128258]

[6]. a)McGee GS, Davidson JM, Buckley A, Sommer A, Woodward SC, Aquino AM, Barbour R, Demetriou AA, J. Surg. Res 1988, 45, 145; [PubMed: 3392988] b)Wang YJ, Shahrokh Z, Vemuri S, Eberlein G, Beylin I, Busch M, in Formulation, Characterization, and Stability of Protein

Drugs: Case Histories, Springer 2002, p. 141;c)Mitchell AC, Briquez PS, Hubbell JA, Cochran JR, Acta Biomater. 2016, 30, 1. [PubMed: 26555377]

[7]. a)Dvorak P, Bednar D, Vanacek P, Balek L, Eiselleova L, Stepankova V, Kunka A, Biotechnol. Bioeng 2018, 115, 850; [PubMed: 29278409] b)Beenken A, Mohammadi M, Nature Rev. Drug Discov 2009, 8, 235. [PubMed: 19247306]

[8]. a)Choi SM, Lee KM, Kim HJ, Park IK, Kang HJ, Shin HC, Baek D, Choi Y, Park KH, Lee JW, Acta Biomater. 2018, 66, 325; [PubMed: 29203426] b)Nguyen TH, Kim S-H, Decker CG, Wong DY, Loo JA, Maynard HD, Nat. Chem 2013, 5, 221. [PubMed: 23422564]

[9]. a)Ha SH, Park TH, Kim S-E, Biotechnol. Tech 1996, 10, 401;b)Ha S, Park T, Biotechnol. Lett 1997, 19, 1087;c)Kim JE, Kim EJ, Rhee WJ, Park TH, Biotechnol. Bioprocess Eng 2005, 10, 353;d)Choi SS, Rhee WJ, Park TH, Biotechnol. Bioeng 2005, 91, 793; [PubMed: 15948145] e)Kim EJ, Park TH, Biotechnol. Bioprocess Eng 2003, 8, 76.

[10]. a)Park HJ, Kim EJ, Koo TY, Park TH, Enzyme Microb. Technol 2003, 33, 466;b)Kim EJ, Rhee WJ, Park TH, Biotechnol. Prog 2004, 20, 324. [PubMed: 14763859]

[11]. a)Rhee WJ, Lee EH, Park TH, Biotechnol. Bioprocess Eng 2009, 14, 645;b)Park JH, Wang Z, Jeong H-J, Park HH, Kim B-G, Tan W-S, Choi SS, Park TH, Appl. Microbiol Biotechnol 2012, 96, 671; [PubMed: 22714097] c)Park JH, Park HH, Choi SS, Park TH, Process Biochem. 2012, 47, 164.

[12]. a)Park JH, Lee JH, Park HH, Rhee WJ, Choi SS, Park TH, Biomaterials 2012, 33, 9127; [PubMed: 22981778] b)Lee HJ, Park HH, Kim JA, Park JH, Ryu J, Choi J, Lee J, Rhee WJ, Park TH, Biomaterials 2014, 35, 1696; [PubMed: 24262100] c)Park HH, Sohn Y, Yeo JW, Park JH, Lee HJ, Ryu J, Rhee WJ, Park TH, Process Biochem. 2014, 49, 1516;d)Park HH, Sohn Y, Yeo JW, Park JH, Lee HJ, Ryu J, Rhee WJ, Park TH, Biotechnol. J 2014, 9, 1582. [PubMed: 25143246]

[13]. Park HH, Woo YH, Ryu J, Lee HJ, Park JH, Park TH, Process Biochem. 2017, 63, 76.

[14]. Ryu J, Kim H, Park HH, Lee HJ, Park JH, Rhee WJ, Park TH, Biotechnol. J 2016, 11, 14

[15]. Plotnikov AN, Hubbard SR, Schlessinger J, Mohammadi M, Cell 2000, 101, 413. [PubMed: 10830168]

[16]. a)Liang CC, Park AY, Guan JL, Nat. Protoc 2007, 2, 329; [PubMed: 17406593] b)Backly RE, Ulivi V, Tonachini L, Cancedda R, Descalzi F, Mastrogiacomo M, Tissue Eng. Part A 2011, 17, 1787; [PubMed: 21385008] c)Carretero M, Escámez MJ, García M, Duarte B, Holguín A, Retamosa L, Jorcano JL, Río M, Larcher F, J. Invest. Dermatol 2008, 128, 223. [PubMed: 17805349]

[17]. Schreier T, Degen E, Baschong W, Res. Exp. Med 1993, 193, 195.

[18]. a)Hirose K, Fujita M, Marui A, Arai Y, Sakaguchi H, Huang YH, Chandra S, Tabata Y, Komeda M, Circ. J 2006, 70, 1190; [PubMed: 16936435] b)Aviles RJ, Annex BH, Lederman RJ, Brit. J. Pharmacol 2003, 140, 637. [PubMed: 14534147]

[19]. Hou YW, Chan MH, Hsu HR, Liu BR, Chen CP, Chen HH, Lee HJ, Exp. Dermatol 2007, 16, 999. [PubMed: 18031459]

[20]. a)An YH, Park MJ, Lee J, Ko J, Kim SH, Kang DH, Hwang NS, Adv. Ther 2020, 3, 1900116;b)Wu F, Yang S, Yuan W, Jin T, Curr. Pharm. Biotechnol 2012, 13, 1292. [PubMed: 22201589]

[21]. Gurtner GC, Werner S, Barrandon Y, Longaker MT, Nature 2008, 453, 314. [PubMed: 18480812]

[22]. a)Choi SM, Ryu HA, Lee KM, Kim HJ, Park IK, Cho WJ, Shin HC, Choi WJ, Lee JW, Biomater. Res 2016, 20, 9; [PubMed: 27042331] b)Ho YC, Mi FL, Sung HW, Kuo PL, Int. J. Pharm 2009, 376, 69; [PubMed: 19450670] c)Mi FL, Shyu SS, Peng CK, Wu YB, Sung HW, Wang PS, Huang CC, J. Biomed. Mater. Res., Part A 2006, 76, 1;d)Xu HL, Tian FR, Lu CT, Xu J, Fan ZL, Yang JJ, Chen PP, Huang YD, Xiao J, Zhao YZ, Sci. Rep 2016, 6, 38332. [PubMed: 27922061]

[23]. Dombkowski AA, Sultana KZ, Craig DB, FEBS Lett. 2014, 588, 206. [PubMed: 24291258]

[24]. Takano K, Okamoto T, Okada J, Tanaka S.-i., Angkawidjaja C, Koga Y, Kanaya S, PLoS One 2011, 6, e16226. [PubMed: 21283826]

[25]. Wu J, Zhu J, He C, Xiao Z, Ye J, Li Y, Chen A, Zhang H, Li X, Lin L, Zhao Y, Zheng J, Xiao J, ACS Appl. Mater. Interfaces 2016, 8, 18710. [PubMed: 27384134]

[26]. Jia X, Tian H, Tang L, Zheng L, Zheng L, Yang T, Yu B, Wang Z, Lin P, Li X, PLoS One 2015, 10, e0117448. [PubMed: 25706539]

[27]. a)Kalluri H, Banga AK, AAPS PharmSciTech 2011, 12, 431; [PubMed: 21369712] b)Pillai O, Nair V, Jain AK, Thomas NS, Panchagnula R, Drug Future 2001, 26, 779.

[28]. a)Benson HAE, Namjosh S, J. Pharm. Sci 2008, 97, 3591; [PubMed: 18200531] b)Chandrasekhar S, Iyer LK, Panchal JP, Topp EM, Cannon JB, Ranade VV, Expert Opin. Drug Delivery 2013, 10, 1155;c)Chaulagain B, Jain A, Tiwari A, Verma A, Jain SK, Artif. Cells, Nanomed., Biotechnol 2018, 46, S472.

[29]. Zheng L, Hui Q, Tang L, Zheng L, Jin Z, Yu B, Wang Z, Lin P, Yu W, Li H, Li X, Wang X, PLoS One 2015, 10, e0135291. [PubMed: 26271041]

[30]. Xu HL, Chen PP, Wang LF, Tong MQ, Cu ZH, Zhao YZ, Xiao J, Fu TL, Wei-Xue, Colloids Surf., B 2018, 172, 573.

[31]. Nasrollahi SA, Taghibiglou C, Azizi E, Farboud ES, Chem. Biol. Drug Des 2012, 80, 639. [PubMed: 22846609]

[32]. Moghadam SH, Saliaj E, Wettig SD, Dong C, Ivanova MV, Huzil JT, Foldvari M, Mol. Pharmaceut 2013, 10, 2248.

[33]. Ulrich MM, Verkerk M, Reijnen L, Vlig M, van den Bogaerdt AJ, Middelkoop E, Wound Repair Regen. 2007, 15, 482. [PubMed: 17650091]

[34]. a)Ferguson MWJ, O'Kane S, Philos. Trans. R. Soc. B 2004, 359, 839;b)Chantre CO, Campbell PH, Golecki HM, Buganza AT, Capulli AK, Deravi LF, Dauth S, Sheehy SP, Paten JA, Gledhill K, Doucet YS, Abaci HE, Ahn S, Pope BD, Ruberti JW, Hoerstrup SP, Christiano AM, Parker KK, Biomaterials 2018, 166, 96. [PubMed: 29549768]

[35]. Tonnesen MG, Feng XD, Clark RAF, J. Invest. Derm. Symp. P 2000, 5, 40.

[36]. Choi HS, Gibbs SL, Lee JH, Kim SH, Ashitate Y, Liu F, Hyun H, Park G, Xie Y, Bae S, Henary M, Frangioni JV, Nat. Biotechnol 2013, 31, 148. [PubMed: 23292608]

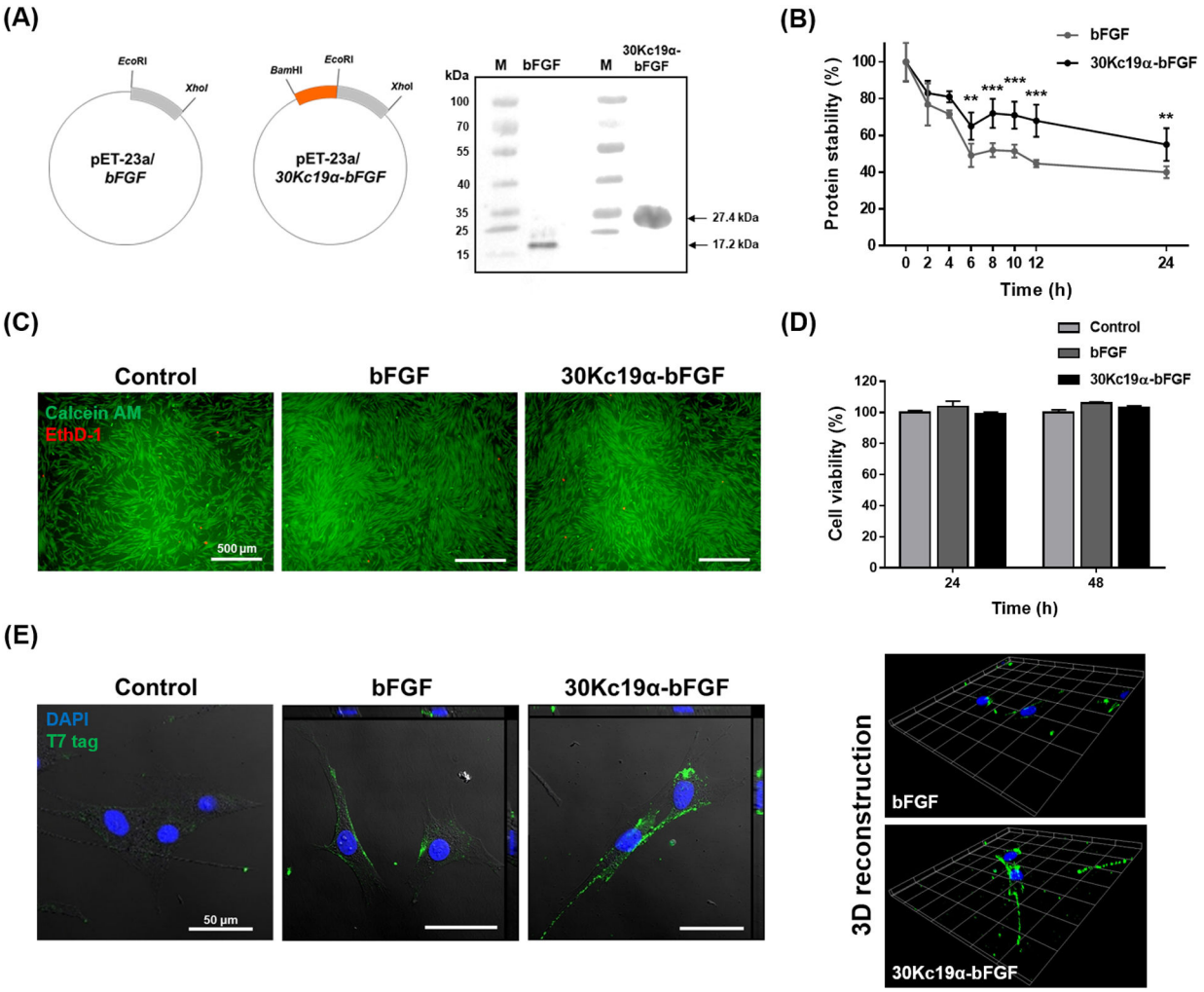

Figure 1. The Fusion of 30Kc19α to bFGF and Its Effects on Stability and Cell-Penetration of bFGF.

(A) Plasmid construction of bFGF and 30Kc19α-bFGF and western blot analysis of recombinant proteins. Anti-T7 tag antibody was used as a primary antibody. (B) Protein stability assay using the bFGF ELISA kit. Proteins at 10 nM were incubated at 37°C from 0 to 24 hours. The relative protein stability was obtained by normalizing protein stability at each time point to protein stability at t = 0 (**$p < 0.01$, ***$p < 0.001$ compared with bFGF group). (C) Cytotoxicity assay using LIVE/DEAD kit and (D) CCK-8 kit. Human dermal fibroblasts (HDFs) were treated with 4 μM of the proteins for 24 and 48 hours. Live and dead cells from 48 hour treated samples were stained with green and red fluorescence respectively (Scale bar=500 μm). CCK-8 assay was done for both 24 and 48 hour treated samples. Data are expressed as relative cell viability normalized to the control group (n=4). (E) Confocal image with orthogonal projection (left) and 3D recostruction of z-stack images (right) of bFGF- and 30Kc19α-bFGF-treated HDFs. HDFs were treated with 4 μM of the proteins for 1 hour. The proteins were tagged with Alexa Fluro® 488, and the nucleus with DAPI (Scale bar = 50 μm).

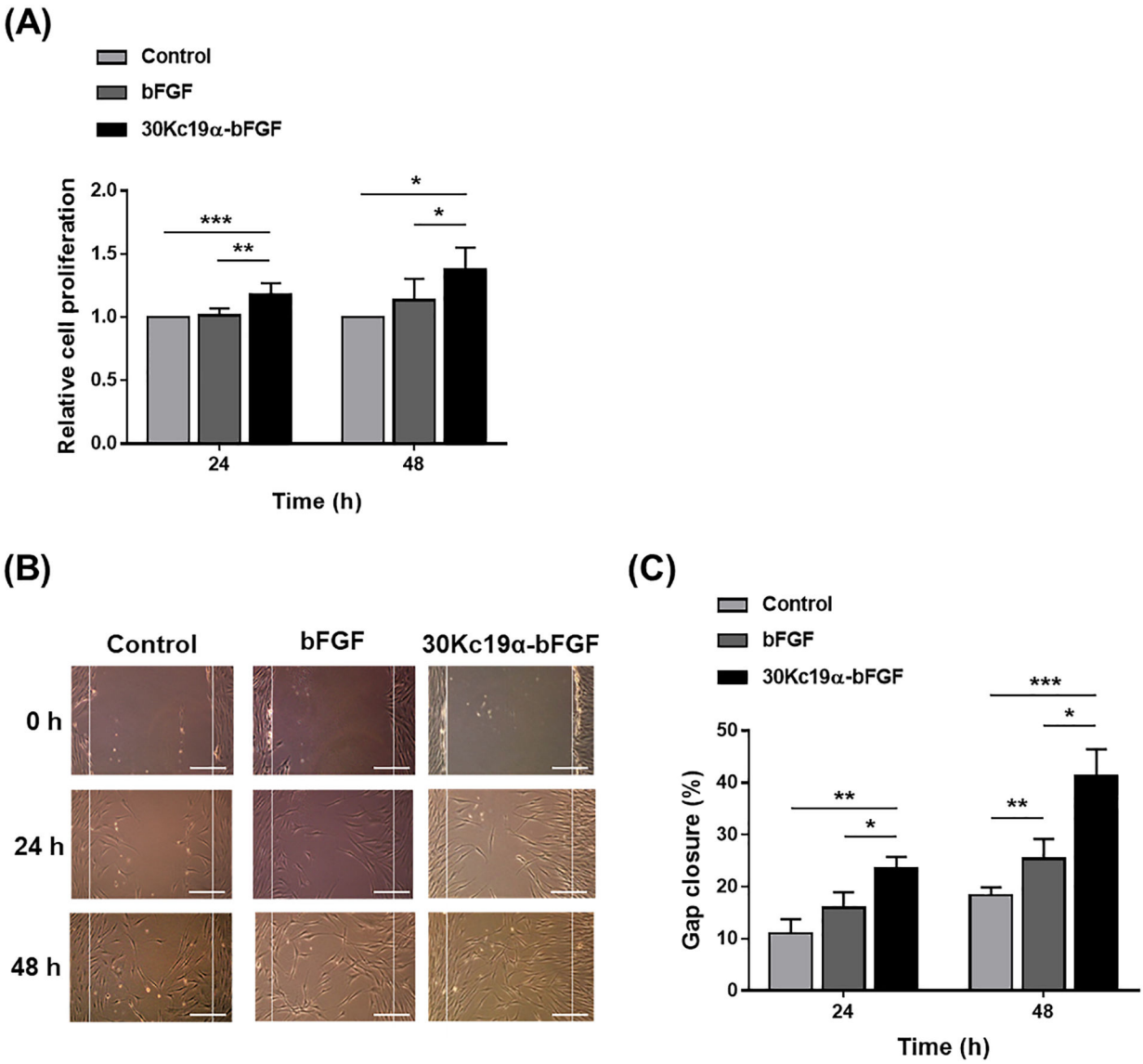

Figure 2. *In Vitro* Wound Healing Effect of 30Kc19α-bFGF on HDFs.

(A) Cell proliferation assay using CCK-8 kit. HDFs were treated with 4 μM of the proteins in serum-free conditions for 24 and 48 hours. Data are expressed as relative cell proliferation normalized to the control group (n=8). (B) *In vitro* wound healing (scratch) assay (Scale bar = 200 μm) and (C) quantification of gap closure in three groups. Gaps were created by scratching the plate using a micropipette tip, and the gap closure was calculated by Equation 1 (n=3) (*p<0.05, **p<0.01, and ***p<0.001).

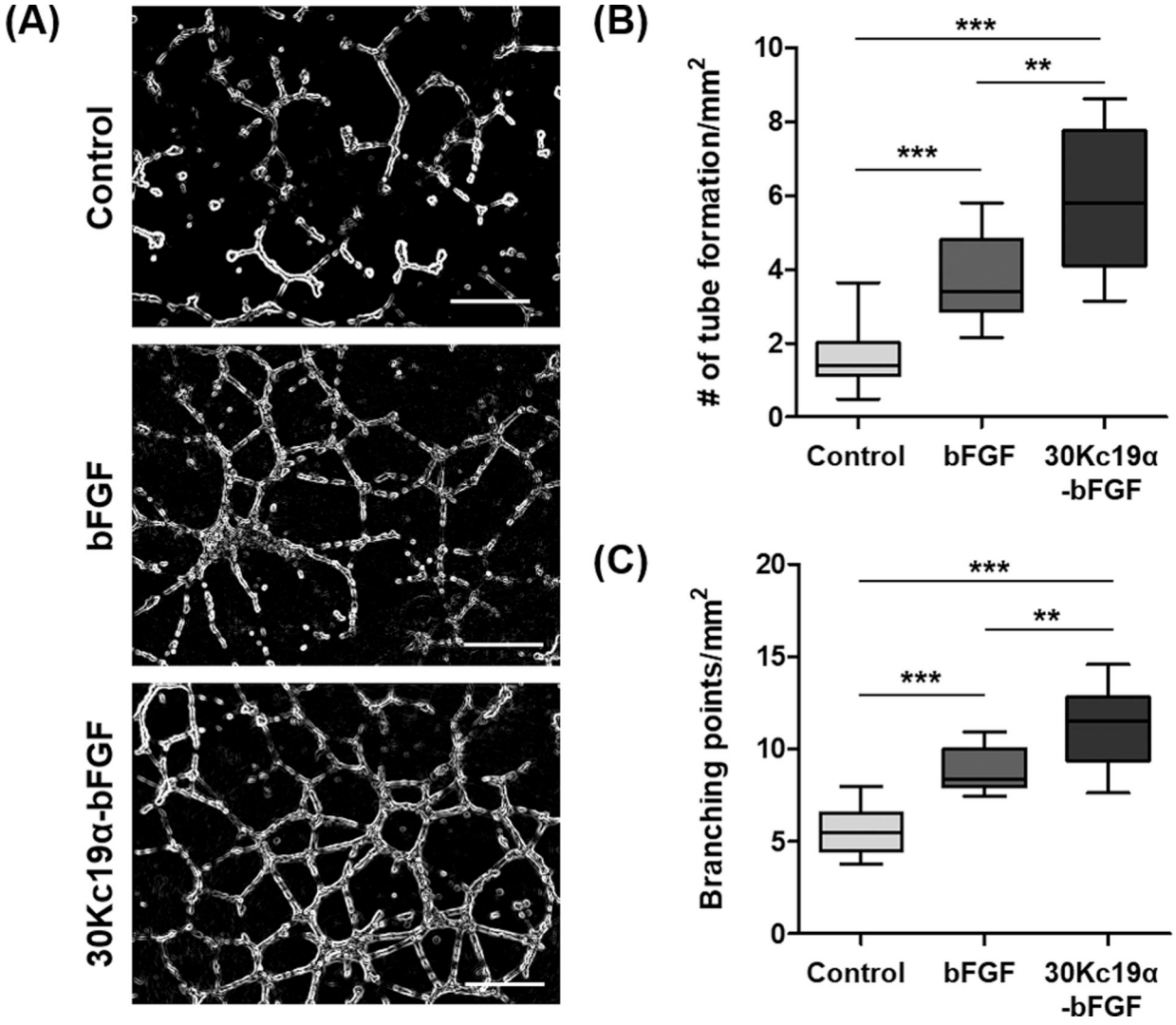

Figure 3. ***In Vitro*** **Angiogenic Effects of 30Kc19α-bFGF on HUVECs.**

(A) Human umbilical vein endothelial cells (HUVECs) formed vasculatures on Matrigel when treated with 4 μM of the proteins for 12 hours (Scale bar=500 μm). Angiogenic effects of 30Kc19α-bFGF were analyzed by measuring (B) the number of tube formation and (C) the count of branching points per unit area based on the microscopic images (n=8–10) (**p<0.01 and ***p<0.001).

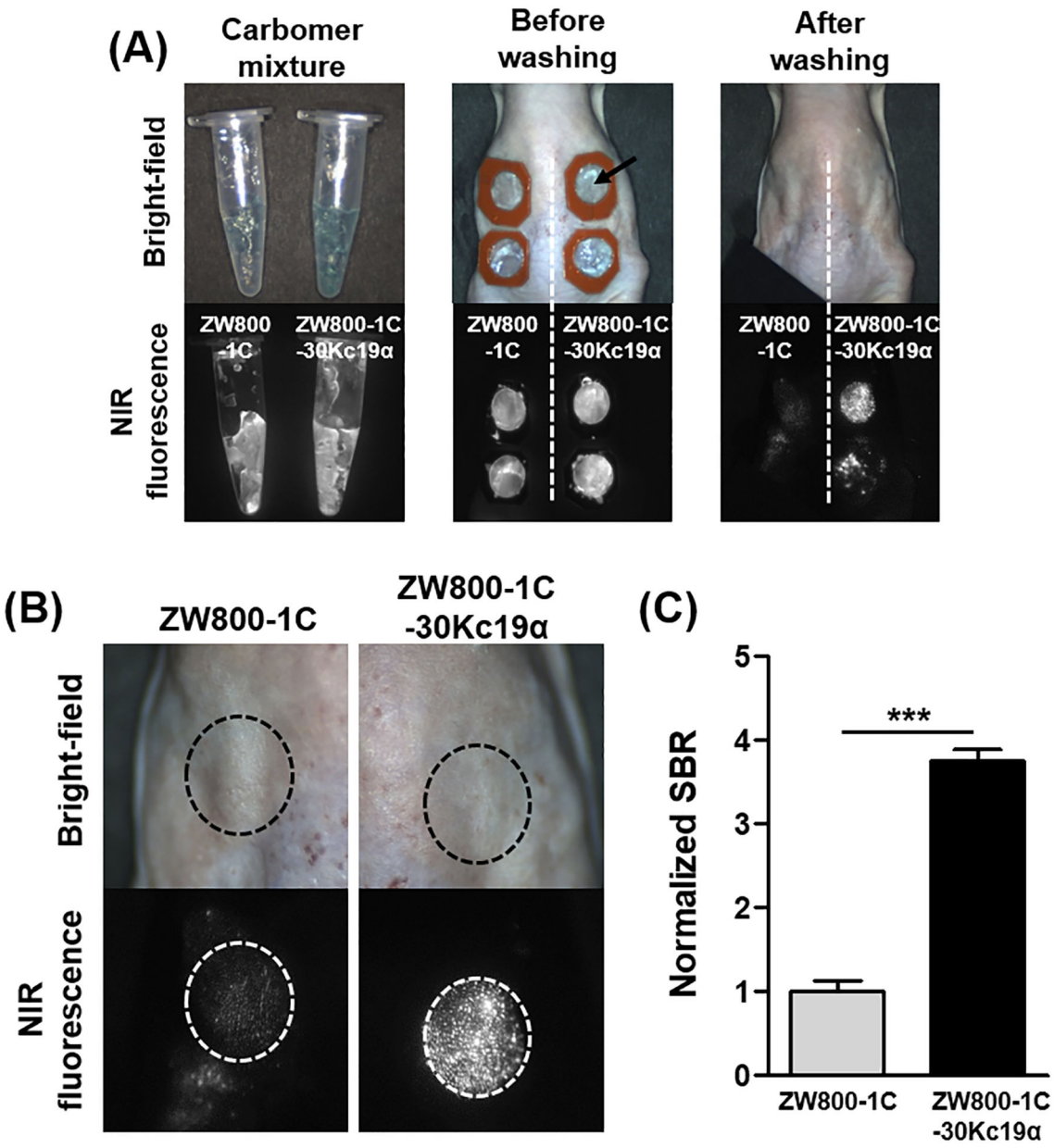

Figure 4. ***In Vivo*** **Skin Penetration Ability of 30Kc19α Using NIR Fluorophore.**

(A) ZW800–1C-30Kc19α conjugate was prepared and applied to the dorsal skin of hairless mice. Images were obtained with the fluorescence-assisted resection and exploration (FLARE) imaging system. (B) Magnified images after washing showed that the ZW800–1C-30Kc19α could penetrate the SC effectively. (C) The fluorescent signal was quantified based on the magnified images, and the normalized signal-to-background ratio (SBR) in ZW800–1C-30Kc19α was significantly higher than that of ZW800–1C, suggesting that 30Kc19α improves the skin penetration ability of small molecules (n=3) (***$p<0.001$).

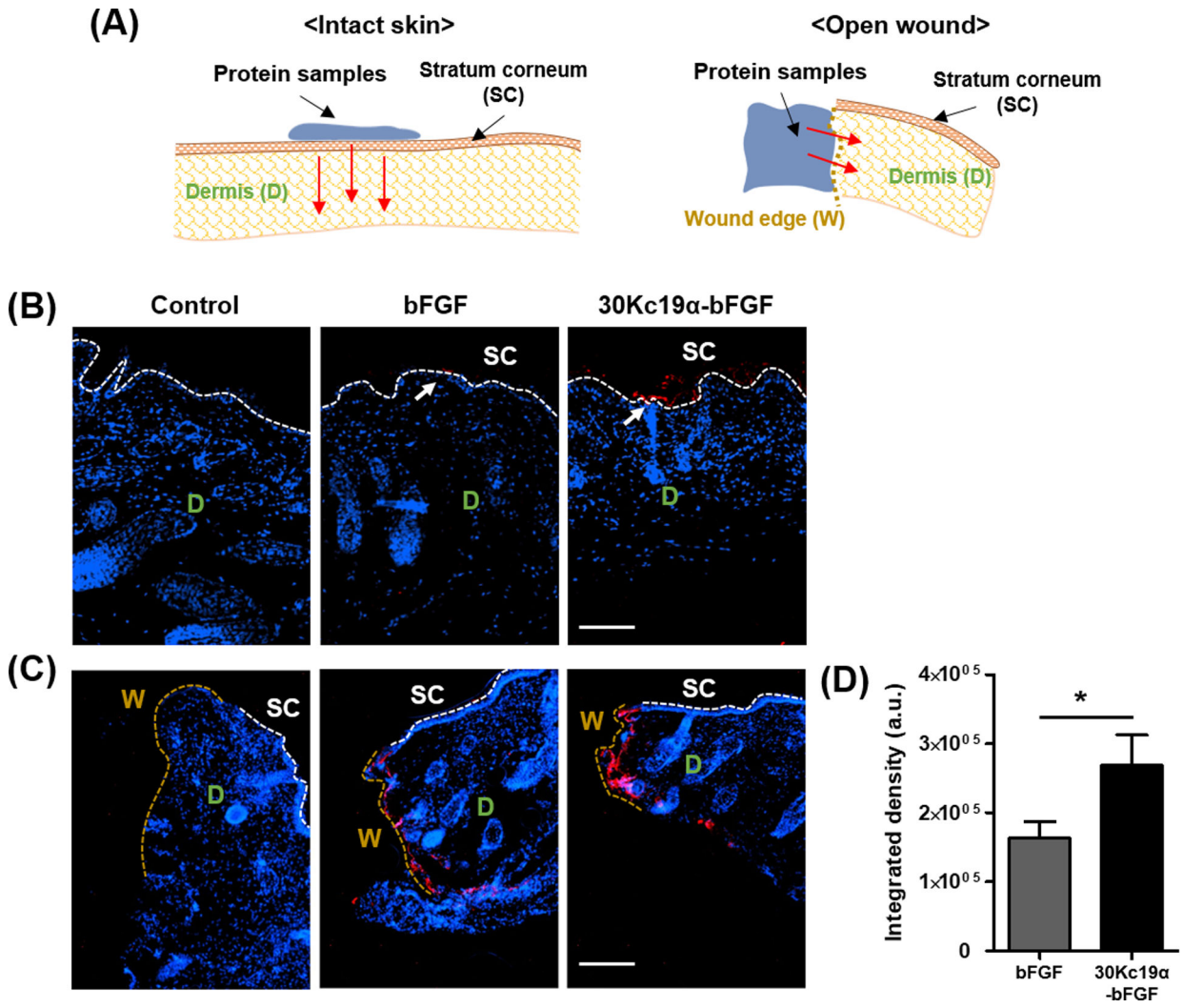

Figure 5. *In Vivo* Transdermal- and Dermal Penetration Ability of 30Kc19α-bFGF.

The transdermal and dermal penetration of 30Kc19α-bFGF on hairless mouse skin was visualized by immunofluorescent staining at 4 hours after application. (A) The experimental scheme showed how the protein samples were applied to the skin and penetrated—the immunofluorescent staining of the proteins in (B) intact skin and (C) open wound cases. 30Kc19α-bFGF exhibited more significant accumulation in the skin tissue than bFGF. (D) The integrated density was measured based on the fluorescent signal in the open wound (n=3–5) (Red arrow: the penetrating direction of proteins) (Scale bar=100 μm).

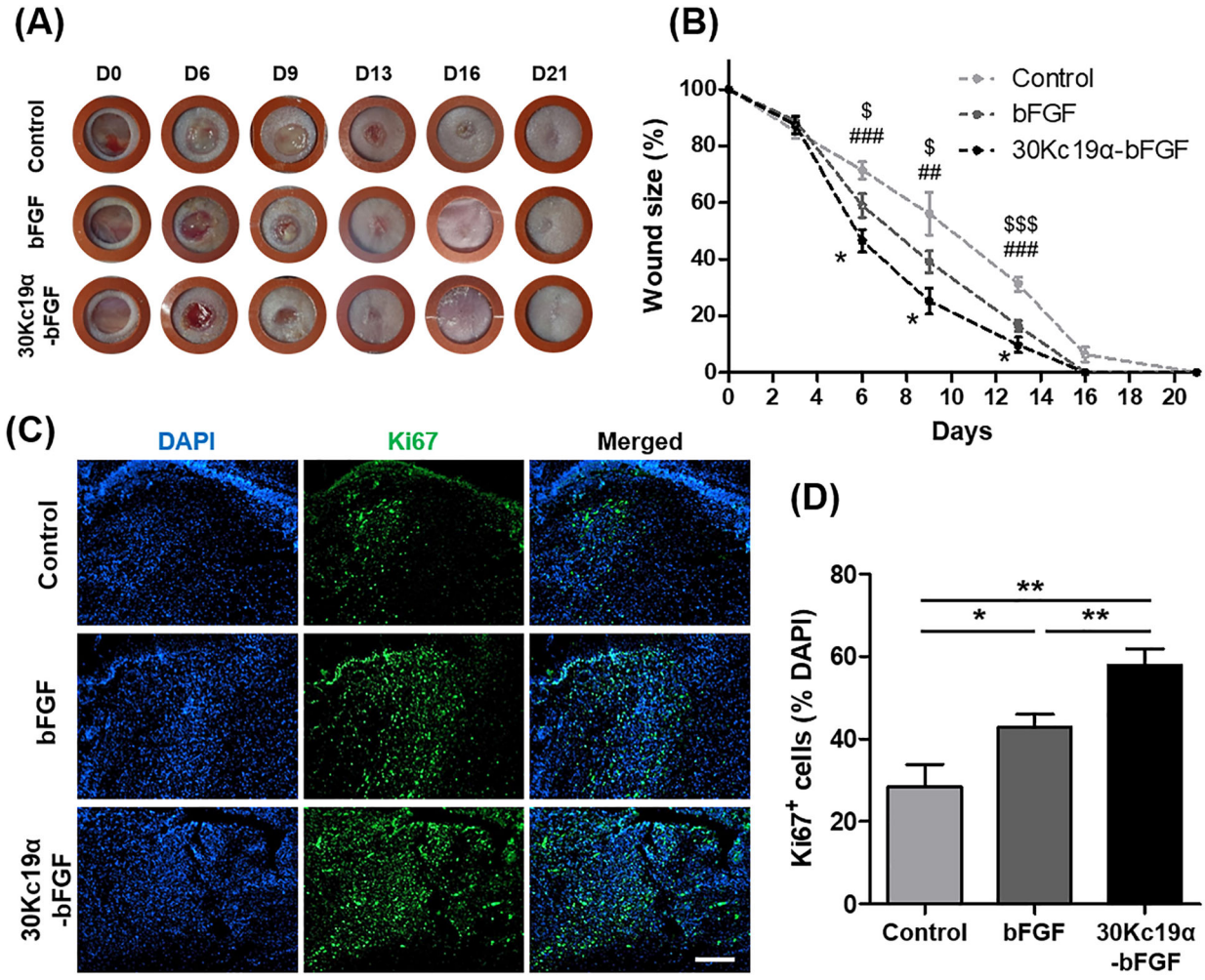

Figure 6. ***In Vivo*** **Wound Healing Application of 30Kc19α-bFGF.**

(A) Photographs of the wound up to 21 days. (B) The wound size-reduction profile was calculated based on the photographs. 30Kc19α-bFGF significantly promoted wound healing compared to bFGF (Statistical significance: * represents 30Kc19α-bFGF to bFGF; # represents 30Kc19α-bFGF to control; and $ represents bFGF to control. $^{*,\$}p<0.05$, $^{\#\#}p<0.01$, and $^{\#\#\#,\$\$\$}p<0.001$). (C and D) Proliferative cells in the wound bed were estimated by immunofluorescence staining of Ki67 (green) on day 6, and quantitatively analyzed based on the fluorescent signals. (Scale bar=200 μm) (n=5–8) ($^{*}p<0.05$ and $^{**}p<0.01$,).

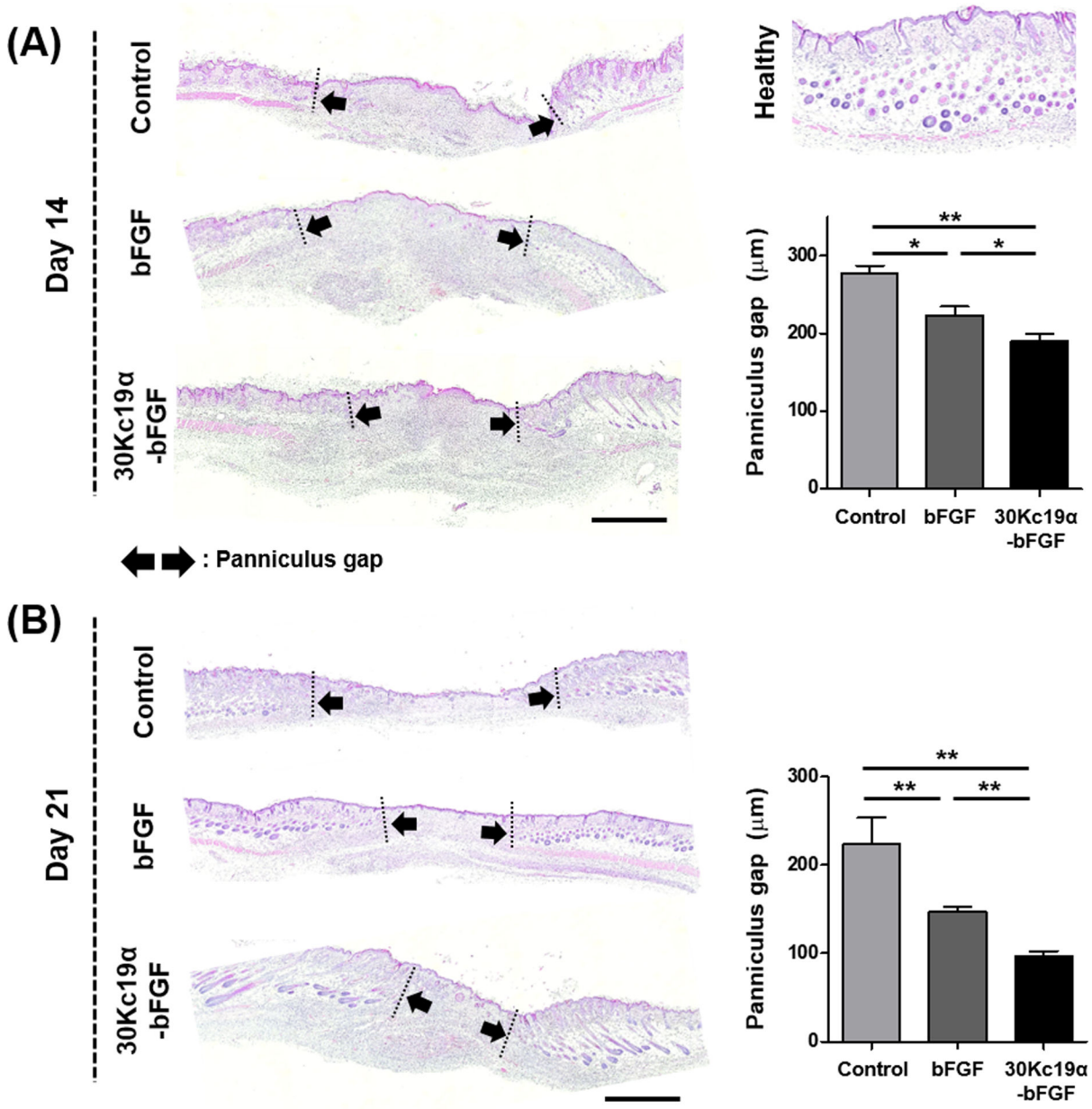

Figure 7. Histological and Qualitative Analysis Based on Hematoxylin and Eosin (H&E) Stain.

Panniculus gap was quantified on day 14 (A) and day 21 (B). It was revealed that 30Kc19α-bFGF accelerated wound regeneration via tissue granulation process. Although the panniculus gap of all groups continuously decreased, it was notably reduced with 30Kc19α-bFGF, whose tissue was being recovered at the fastest rate with a structure similar to healthy tissue (Scale bar=1 mm) (n=3–4) (*p<0.05 and **p<0.01).

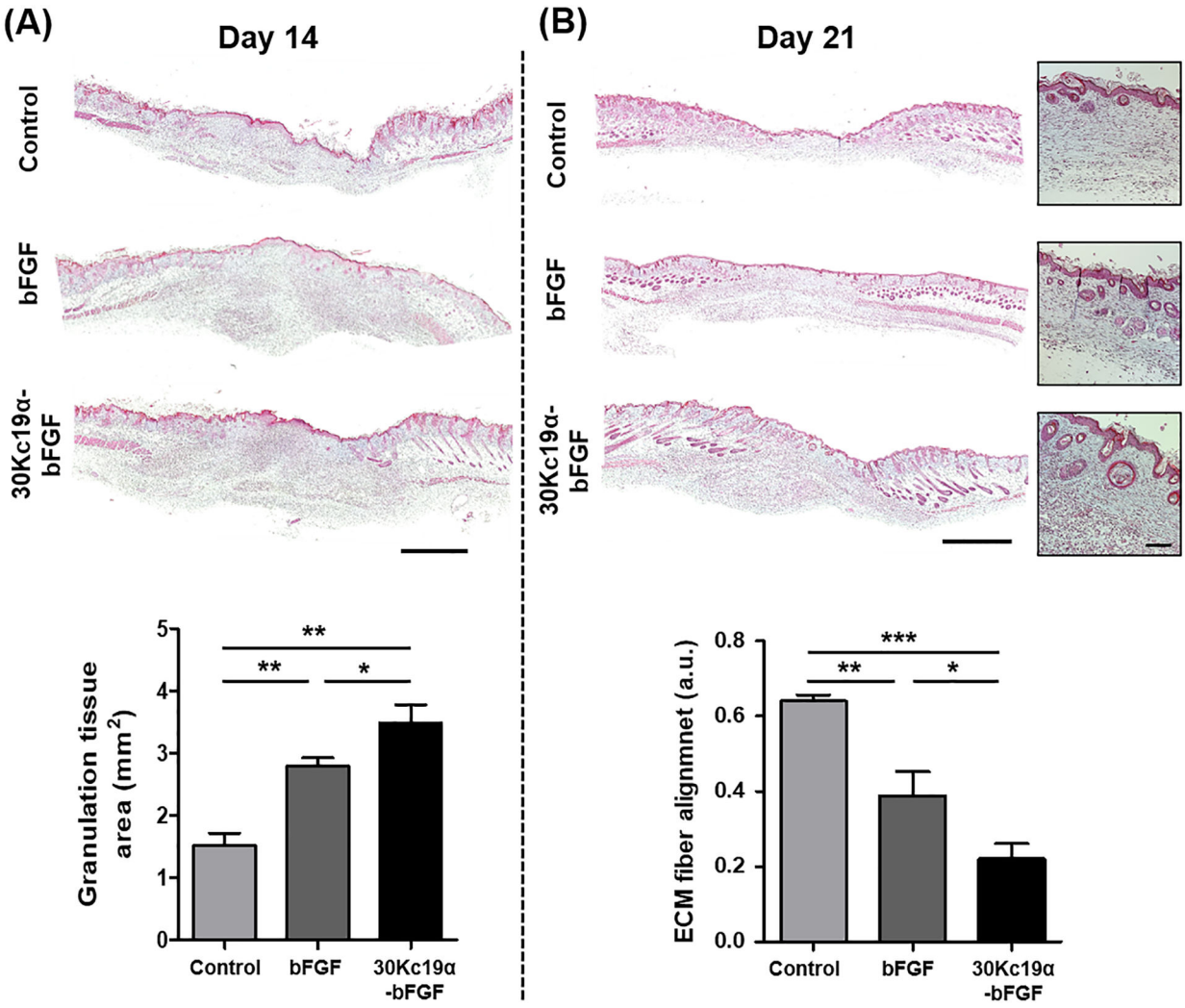

Figure 8. Histological and Qualitative Analysis Based on Masson's Trichrome (MTC) Stain.

Tissue granulation and the degree of extracellular matrix (ECM) fiber alignment were analyzed by MTC staining of the skin tissue on day 14 (A) and day 21 (B), respectively. It was confirmed that 30Kc19α-bFGF supported tissue granulation during the proliferative phase of the wound healing process. Also, both collagen deposition and the formation of skin appendages were enhanced in 30Kc19α-bFGF on day 21. The organization of ECM fiber alignment was quantified at the dermis layer, where the value represents its coherence. 30Kc19α-bFGF exhibited better results all round (Scale bar=1 mm and 100 μm in low and high magnified images, respectively) (n=3–4) (*p<0.05, **p<0.01, and ***p<0.001).

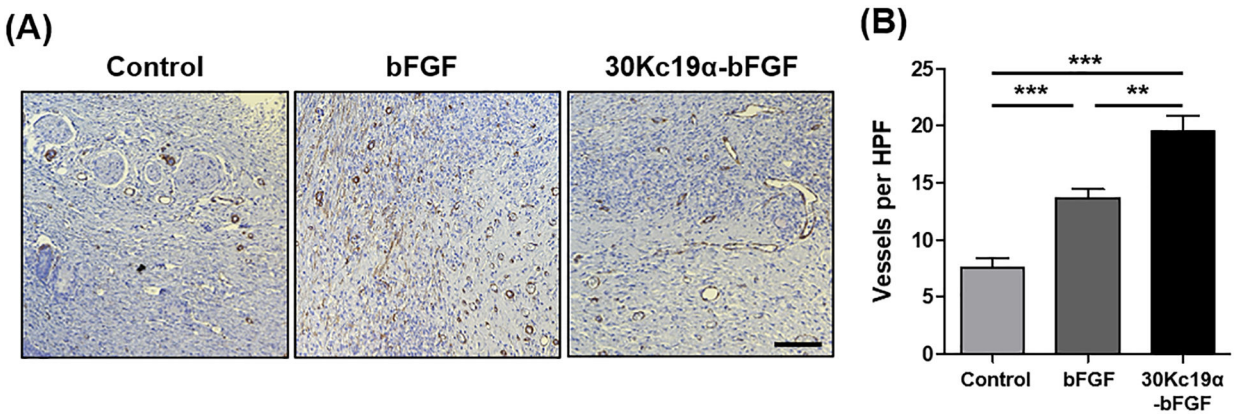

Figure 9. ***In Vivo*** **Angiogenic Ability of 30Kc19α-bFGF.**

(A) Immunohistochemistry staining of alpha-smooth muscle actin (α-SMA) on day 14 and (B) its quantitative analysis. 30Kc19α-bFGF improved angiogenesis during wound healing compared to control and bFGF and newly formed vessels had enlarged and stretched structures (Scale bar=100 μm) (n=10–15) (**p<0.01 and ***p<0.001).